Kinetic Stress and Intrinsic Flow in a Toroidal Plasma

W. X. Ding,[1,3] L. Lin,[1] D. L. Brower,[1,3] A. F. Almagri,[2,3] B. E. Chapman,[2] G. Fiksel,[3] D. J. Den Hartog,[2,3] and J. S. Sarff[2,3]

[1]*Department of Physics and Astronomy, University of California Los Angeles, Los Angeles, California 90095, USA*
[2]*Physics Department, University of Wisconsin, Madison, Wisconsin 53706, USA*
[3]*Center for Magnetic Self-Organization in Astrophysical and Laboratory Plasmas, University of Wisconsin,
Madison, Wisconsin 53706, USA*

A new mechanism for intrinsic plasma flow has been experimentally identified in a toroidal plasma. For reversed field pinch plasmas with a few percent β (ratio of plasma pressure to magnetic pressure), measurements show that parallel pressure fluctuations correlated with magnetic fluctuations create a kinetic stress that can affect momentum balance and the evolution of intrinsic plasma flow. This implies kinetic effects are important for flow generation and sustainment.

Plasma flow and momentum transport are of great interest in both astrophysical and laboratory plasmas. Momentum transport in a hot accretion disk must be much faster than allowed by classical dissipation. Rapid angular momentum transport is attributed to fluctuation-induced stresses, such as the Maxwell and Reynolds stresses, arising from the magneto-rotational instability predicted by magneto-hydrodynamic (MHD) theory [1]. Anomalous momentum transport and intrinsic plasma parallel flow (spontaneous flow without momentum input) are also observed in toroidal magnetic confinement devices such as the tokamak and reversed-field pinch (RFP) [2,3]. It has been demonstrated that flow and flow shear can act to suppress both MHD instabilities [4] and microturbulence [5]. Furthermore, the application of resonant helical magnetic perturbations in the edge of tokamak plasmas can drive plasma flow, in addition to suppressing edge instabilities [6]. Understanding the complex physics of intrinsic flow and momentum transport due to electromagnetic fluctuations is likely to play a critical role in future burning plasma devices like ITER where the external neutral beams may be unable to drive sufficient plasma flow to control instabilities [7].

In this Letter, we report on the first measurement of the fluctuation-induced kinetic stress resulting from the correlated product of density fluctuations and radial magnetic field fluctuations in the core of a high-temperature reversed field pinch plasma. Measurements reveal that the force density associated with the kinetic stress is directed to accelerate the plasma between magnetic relaxation events in a manner consistent with observed intrinsic flow. These results imply kinetic effects are important for momentum transport and plasma flow in finite β (ratio of plasma pressure to magnetic pressure) plasmas.

Self-generation of plasma flow bears similarity to self-generation of a magnetic field as described in mean-field dynamo theory. Momentum transport and physics of flow generation in plasmas are captured by the momentum balance equation

$$\rho\left(\frac{\partial \vec{V}}{\partial t} + \vec{V} \bullet \nabla \vec{V}\right) = \vec{J} \times \vec{B} - \nabla \bullet \overset{\leftrightarrow}{P} + \mu \nabla^2 \vec{V}, \quad (1)$$

where $\rho = n_e M$ is the plasma mass density, n_e is electron density (equivalent to ion density), M is ion mass, and $\overset{\leftrightarrow}{P}$ is the pressure tensor. $\vec{J}$, $\vec{V}$, $\vec{B}$, μ are the plasma current density, velocity, magnetic field, and viscosity coefficient, respectively. In the absence of external forces, large-scale plasma flow is affected by spatial (and possibly temporal) fluctuations in the various fields contained in Eq. (1). To illustrate the turbulent mechanisms, the equation for the momentum flux parallel to the mean field and associated with correlated fluctuating quantities is constructed. Each quantity is decomposed into mean and fluctuating parts (e.g., $\vec{J} = \vec{J}_0 + \delta\vec{J}$, $\vec{B} = \vec{B}_0 + \delta\vec{b}$), and an ensemble average yields

$$\rho \frac{\partial \langle V_\parallel \rangle}{\partial t} = \mu \nabla^2 \langle V_\parallel \rangle - \rho \langle \delta\vec{V} \bullet \nabla \delta\vec{V} \rangle_\parallel + \langle \delta\vec{J} \times \delta\vec{b} \rangle_\parallel$$
$$- \nabla \bullet \frac{\langle \delta p_\parallel \delta b_r \rangle}{B} \vec{e}_r, \quad (2)$$

where δ denotes a fluctuating quantity, and $\langle \ldots \rangle$ refers to a mean or ensemble-averaged quantity that corresponds to a local magnetic flux surface average. The subscript "$\parallel$" indicates the component parallel to $\vec{B}_0$, and $\vec{e}_r$ is a radial unit vector. On the right-hand side, the first term represents damping due to viscosity. The mean flow (left-hand side) can be affected by three fluctuation-induced force terms (last three terms on the right-hand side): (1) Reynolds stress, (2) Maxwell stress (closely related to the Hall dynamo in Ohm's law), and (3) kinetic stress resulting from the correlation between parallel pressure and magnetic fluctuations, respectively. The magnetic fluctuation-induced kinetic stress in Eq. (2) arises from the projection of the parallel momentum flux along the radial direction in a toroidal device [8],

$$\Pi = \langle p_\parallel \vec{b} \bullet \vec{e}_r \rangle, \tag{3}$$

where $p_\parallel$ is the parallel momentum flux, $\vec{b} = \vec{B}/B$ is a unit vector parallel to $\vec{B}$. Both the parallel momentum flux and magnetic field can be decomposed into mean and fluctuating components, i.e., $p_\parallel = p_{\parallel,0} + \delta p_\parallel$, $B_r = B_{r0} + \delta b_r$, and $\delta p_\parallel = T_\parallel \delta n_e + n_e \delta T_\parallel$, leading to

$$\Pi = \frac{\langle \delta p_\parallel \delta b_r \rangle}{B} = T_\parallel \frac{\langle \delta n_e \delta b_r \rangle}{B} + n_e \frac{\langle \delta T_\parallel \delta b_r \rangle}{B}$$
$$= \Pi^n + \Pi^T, \tag{4}$$

where δb_r is radial magnetic fluctuations, $T_\parallel$ is plasma parallel temperature, and $\langle B_{r0} \rangle = 0$. Note that Π^n depends on density fluctuations and Π^T depends on temperature fluctuations correlated with δb_r. In this work, only the kinetic stress $-\nabla \bullet \langle \Pi^n \vec{e}_r \rangle$ associated with density fluctuations is directly measured.

Measurements were carried out on the Madison Symmetric Torus (MST) RFP with major radius $R_0 = 1.5$ m, minor radius $a = 0.52$ m, discharge current $I_p = 350$–400 kA, line-averaged density $\bar{n}_e \sim 1 \times 10^{19}$ m^{-3}, and temperature $T_e \sim T_i \sim 300$ eV for deuterium plasmas [9]. The deuterium ion temperature and poloidal flow are measured by Rutherford scattering [10]. The core plasma flow velocity can also be inferred from the magnetic mode rotation speed, which is consistent with spectroscopic measurements [3]. A high-speed (~ 4 μs), laser-based (432 μm), polarimeter-interferometer system with 11 vertically viewing chords (separation ~ 8 cm) is employed for the measurement of kinetic stress. A fluctuating magnetic field is obtained from Faraday-effect polarimetry, and an interferometer-differential interferometer system allows us to measure density fluctuations and their gradient [11,12]. Here we primarily focus on flow dynamics and kinetic stress away from transient sawtooth crash events and during sawtooth-free high-confinement plasma discharges achieved by using a pulsed-poloidal-current drive (PPCD), an inductive technique employed to reduce tearing instability [13].

Typical MST discharges exhibit a quasiperiodic relaxation oscillation (sawtooth cycle) in many plasma parameters, e.g., density, temperature, and current density. During current flat top, $t = 10$–30 ms in Fig. 1(a), the innermost-resonant core tearing mode $(m, n) = (1, 6)$, driven unstable by the radial current density gradient, also displays a sawtoothing behavior [Fig. 1(b)]. Here (m,n) refer to the poloidal and toroidal mode numbers, respectively. In contrast, the (0,1) tearing mode, resonant at the reversal surface near the plasma edge ($r/a \sim 0.8$), surges only at the crash event [Fig. 1(c)]. Correspondingly, plasma flow in the core displays a similar sawtooth cycle as shown in Fig. 1(d). The observed flow is always in the direction of the plasma current (co-current) in the core. The flow direction relative to the magnetic field depends on the initial vacuum toroidal field that is counter to the current
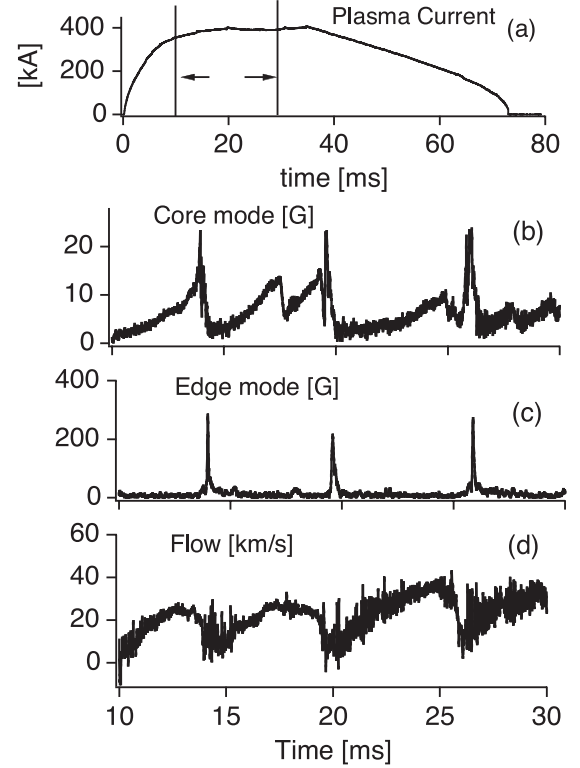
FIG. 1. (a) Discharge current; (b) core resonant tearing mode $(m/n = 1/6)$ activity; (c) edge resonant tearing mode $(m/n = 0/1)$ activity; and (d) core mode rotation velocity for shot 1 060 818 084. Sawtooth crashes occur at ~ 15, 20, and 25 ms.

for this study. Temporal evolution of plasma flow exhibits a slow growth phase, often followed by saturation and then rapid relaxation at the sawtooth crash. These data evidence a strong correlation between flow dynamics and tearing mode activity. Intrinsic plasma flow is redistributed when the edge (0,1) tearing mode surges and within ~ 100 μs momentum is transported outward during magnetic reconnection [3]. The mean parallel flow profile, ($V_\parallel = \vec{V} \bullet \vec{B}/B_0$), derived from a combination of the measured plasma flow, magnetic mode velocities, and the equilibrium magnetic field is shown in Fig. 2(a), at ~ 1 ms prior to a crash. In the plasma interior, parallel flow is negative (i.e., opposing the local magnetic field direction) and slowly decreasing to zero near midradius, $r/a \sim 0.5$. Outside this radius, the plasma flow reverses sign and increases toward the edge. This spatial distribution supports global momentum conservation inside the plasma volume surrounded by a close-fitting conducting shell. However, the origin or drive of intrinsic plasma flow remains unknown since there is no external momentum input.

Line-integrated density and Faraday effect fluctuation measurements for the core resonant (1,6) mode are plotted in Figs. 3(a) and 3(b), respectively. For global tearing instabilities of known mode number, the density and magnetic field fluctuation spatial profiles can be obtained by
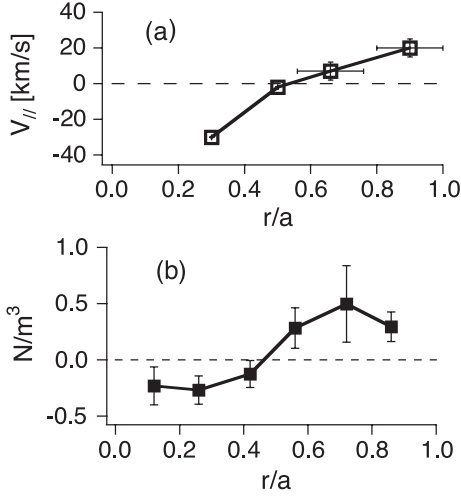
FIG. 2.   (a) Mean parallel flow profile at $t = 1$ ms before sawtooth crash. Negative sign indicates that flow is opposite to magnetic field direction. (b) Time-averaged kinetic stress $(-\nabla \bullet \langle \Pi^n \vec{e}_r \rangle)$ at $t = 1$ ms before sawtooth crash summed over modes $m = 1$, $n = 6$–15.

inversion using a minimization procedure as described elsewhere [14]. The local mode amplitude profiles are depicted in Figs. 3(c) and 3(d), for density and magnetic (radial and poloidal) fluctuations, respectively. Density fluctuations vanish at the magnetic axis, reach a maximum near the location of the peak equilibrium density gradient, and then decrease towards the boundary. As expected, radial magnetic fluctuations associated with tearing modes peak in the core at the mode resonant surface and monotonically decrease to zero at the boundary. Poloidal
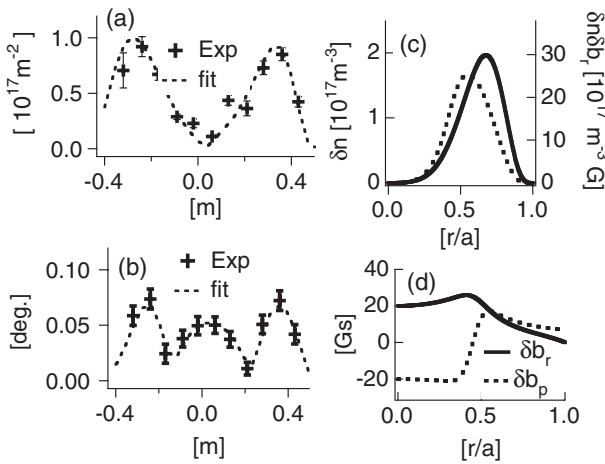
FIG. 3.   Measured line-integrated (a) density fluctuation profile (cross) for $m/n = 1/6$ tearing mode. (b) Faraday rotation fluctuation (cross) profile. Best fits from inversion are represented by dashed line. (c) Local density fluctuations profile for $m/n = 1/6$ tearing mode; dashed line is product $|\delta n_e \delta b_r|$. (d) Radial and poloidal magnetic fluctuation profiles for $m/n = 1/6$ tearing mode. Modes with $m = 1$ and $n = 7$–15 have similar profiles.

magnetic field fluctuations are zero at the resonant surface, peaking on either side with opposite sign. The product, $|\delta n_e \delta b_r|$, has a maximum near the midradius as shown in Fig. 3(c). Dashed lines in Figs. 3(a) and 3(b) are derived by computing line integrals of the local profiles and represent a best fit to the data.

The kinetic stress $(-\nabla \bullet \langle \Pi^n \vec{e}_r \rangle)$ direction, amplitude, and spatial distribution are shown in Fig. 2(b). The correlated product of density fluctuations and radial magnetic field fluctuations is achieved by ensemble averaging over more than 700 similar events and summed for modes $m = 1$, $n = 6$–15. In the plasma core, the kinetic stress is about -0.25 N/m³ and reverses sign near half radius, reaching a maximum 0.5 N/m³ towards the edge. The kinetic force, which does not depend explicitly on plasma flow, tends to drive plasma flow with a spatial distribution and direction similar to the observed parallel flow. As shown in Fig. 3(c), the product of density and radial magnetic fluctuations peaks in the plasma interior and its derivative goes to zero at $r/a \sim 0.5$. Hence, the kinetic stress vanishes there. Positive and negative kinetic stresses act to drive a sheared plasma flow.

Plasma parallel flow dynamics, as seen in Fig. 1(d), can be divided into three phases: flow ramp-up, saturation, and crash. First, during the flow ramp-up phase, kinetic stress $(-\nabla \bullet \langle \Pi^n \vec{e}_r \rangle)$ is negative in the core and tends to drive more negative flow $(\rho \partial V_\parallel / \partial t < 0)$ as observed. As shown in Fig. 1(d), the flow increase between sawteeth (20–25 ms) is $|\Delta V_\parallel| \approx 33$ km/s. An estimate of the flow generation rate is $\rho \Delta V_\parallel / \Delta t \approx -0.20$ N/m³. This force is comparable to the measured kinetic stress $(-0.25 \pm 0.1$ N/m³) at $r/a = 0.26$ as shown in Fig. 2(c). These measurements indicate that the kinetic stress is large enough to generate the observed flow, assuming other fluctuation-induced forces are ignorable.

Second, during the flow saturation phase $(\rho \partial V_\parallel / dt \approx 0)$ [Fig. 2(a)], the kinetic stress must be balanced by dissipation, presumably turbulent since classical dissipation (250 ms) is much longer than the discharge duration. For transport analysis Eq. (2) can be written phenomenologically as

$$\rho \frac{\partial \langle V_\parallel \rangle}{\partial t} = -\nabla \bullet (\Pi_{\parallel,r} \vec{e}_r)$$

$$\Pi_{\parallel,r} = -\rho D^T \frac{\partial \langle V_\parallel \rangle}{\partial r} + \rho V_{\text{pinch}} \langle V_\parallel \rangle + R_s \tag{5}$$

where D^T is turbulence-driven diffusivity, V_{pinch} is turbulence-driven pinch, and R_s is the residual stress that may arise from Reynolds stress, Maxwell stress, or kinetic stress [15]. The pinch term results from toroidal effects, important for tokamak plasmas owing to the strong toroidal magnetic field [16]. While the pinch term has not been analyzed for the RFP, it is assumed small given that the poloidal magnetic field is dominant.

To be near stationary, the flow gradient (diffusive term) must be sustained by residual stresses. In standard MST plasmas for which the magnetic field is expected to be stochastic, previous transient transport experiments using biased electrodes revealed that the momentum confinement time is approximately equal to energy confinement time (1–2 ms) [17] for the between crash phase, consistent with quasilinear theory [18]. The turbulent diffusivity is approximately $D^T \approx D_m V_{i,\mathrm{th}} \sim 5.0 \ \mathrm{m}^2/\mathrm{s}$ using measured plasma parameters, where $D_m \sim 0.5 \times 10^{-4}$ m is the magnetic field line diffusion coefficient [19] determined from field line tracing [20] and $V_{i,\mathrm{th}}$ is the ion thermal speed. With this information we can evaluate the diffusive term $\rho D^T \frac{\Delta V_\parallel}{\Delta r} \sim (2.0 \pm 1.0) \times 10^{-2} \ \mathrm{N/m}^2$ [see Fig. 2(a)], which depends explicitly on flow. In addition, from Fig. 2(b), we estimate $\Pi^n \approx (r/2)\nabla \bullet (\Pi^n \vec{e}_r) \approx 1.8 \times 10^{-2} \ \mathrm{N/m}^2$ at $r/a = 0.26$ in the core. The measured Π^n is comparable in magnitude to the stochastic field diffusion that provides a flow saturation mechanism. Therefore, the kinetic stress can generate flow ($\rho \partial \langle V_\parallel \rangle / \partial t \neq 0$), when stochastic field diffusion is negligible due to low initial velocity, and sustain flow at saturation ($\rho \partial \langle V_\parallel \rangle / \partial t = 0$) when the kinetic stress is balanced by stochastic field diffusion.

Third, during a sawtooth crash phase, momentum transport is even faster (within 100 μs) than that expected from stochastic magnetic field diffusion [14]. This fast momentum transport is likely the result of very large Maxwell and Reynolds stresses when significant three-wave nonlinear coupling among tearing modes occurs as reported in Ref. [21].

On MST, magnetic fluctuations can be controlled by deliberately applying inductive PPCD, which alters the current density profile to suppress tearing activity. This results in dramatically improved particle and energy confinement leading to tokamak-like confinement [13]. As shown in Fig. 4(a), intrinsic flow shows an increase at the onset of PPCD at about 10 ms, reaches a maximum of 27 km/s at $t = 13$ ms, and then gradually decreases to ~13 km/s at $t = 20$ ms. Plasma temperature (and density) reach their maximum value at $t \sim 18$ ms. During this time, both core tearing mode and line-averaged density fluctuations [Fig. 4(b)] track the parallel plasma flow dynamics, further indicating a strong correlation between intrinsic flow and fluctuations. The time-averaged (between 15 and 20 ms) kinetic stress measurement during PPCD is shown in Fig. 4(c). The kinetic stress profile at peak confinement (15–20 ms) is similar to that in standard plasmas but ten times smaller due to the suppression of tearing activity. Both kinetic stress and stochastic magnetic field diffusion are greatly suppressed during high-confinement PPCD plasmas. The observed flow decay in Fig. 4(a) may be associated with electrostatic turbulence as is thought to be the case for tokamaks [15].

Momentum transport and plasma flow from current-driven tearing instabilities in RFP plasmas have been
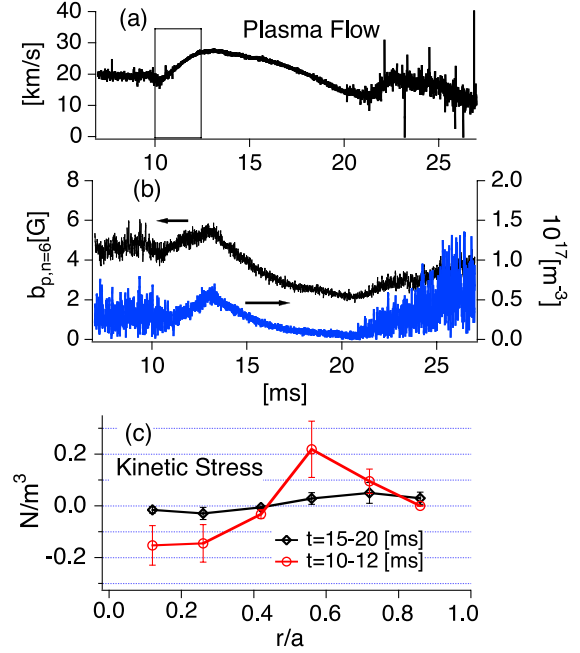
FIG. 4 (color online).   (a) Core plasma parallel flow, and (b) (1,6) tearing mode magnetic and line-averaged density fluctuations at $r/a = 0.5$ during PPCD ($10 < t < 20$ ms). (c) Kinetic stress profile for time intervals 10–12 ms (circles) and 15–20 ms (diamonds).

investigated computationally using MHD [22] and non-reduced MHD equations [23]. It was found that the Reynolds and Maxwell stresses are large and tend to oppose each other as observed in the edge of MST plasmas. Nevertheless, experimentally establishing the existence of the kinetic stress in moderate β plasmas emphasizes that kinetic effects beyond MHD, and its two-fluid extensions are required to fully understand intrinsic plasma rotation and momentum transport.

In summary, the first direct measurement of magnetic-fluctuation-induced kinetic stress has been made in the core of a high-temperature plasma. The observed kinetic stress acts as a force driving plasma flow and can be balanced by stochastic magnetic-field-induced momentum diffusion to sustain a near stationary parallel flow.

[1] S. A. Balbus and J. F. Hawley, Rev. Mod. Phys. **70**, 1 (1998).
[2] J. E. Rice *et al.*, Phys. Rev. Lett. **106**, 215001 (2011).
[3] S. C. Prager *et al.*, Plasma Phys. Controlled Fusion **37**, A303 (1995); D. J. Den Hartog, J. T. Chapman, D. Craig, G. Fiksel, P. W. Fontana, S. C. Prager, and J. S. Sarff, Phys. Plasmas **6**, 1813 (1999).
[4] E. J. Strait, T. Taylor, A. Turnbull, J. Ferron, L. Lao, B. Rice, O. Sauter, S. Thompson, and D. Wróblewski, Phys. Rev. Lett. **74**, 2483 (1995).

[5] T. S. Hahm, Phys. Plasmas **1**, 2940 (1994).

[6] T. E. Evans *et al.*, Phys. Rev. Lett. **92**, 235003 (2004); T. E. Evans *et al.*, Nucl. Fusion **48**, 024002 (2008); K. H. Finken *et al.*, Phys. Rev. Lett. **94**, 015003 (2005).

[7] K. Ikeda, Nucl. Fusion **47**, E01 (2007).

[8] S. C. Prager, Plasma Phys. Controlled Fusion **41**, A129 (1999).

[9] R. N. Dexter *et al.*, Fusion Technol. **19**, 131 (1991).

[10] J. C. Reardon, G. Fiksel, C. B. Forest, A. F. Abdrashitov, V. I. Davydenko, A. A. Ivanov, S. A. Korepanov, S. V. Murachtin, and G. I. Shulzhenko, Rev. Sci. Instrum. **72**, 598 (2001).

[11] W. X. Ding, D. L. Brower, and T. Y. Yates, Rev. Sci. Instrum. **79**, 10E 701 (2008).

[12] W. X. Ding, D. Brower, G. Fiksel, D. J. Den Hartog, S. Prager, and J. Sarff, Phys. Rev. Lett. **103**, 025001 (2009).

[13] J. S. Sarff, N. E. Lanier, S. C. Prager, and M. R. Stoneking, Phys. Rev. Lett. **78**, 62 (1997); B. E. Chapman *et al.*, Phys. Rev. Lett. **87**, 205001 (2001); J. S. Sarff *et al.*, Nucl. Fusion **43**, 168 (2003).

[14] W. X. Ding, D. L. Brower, D. Craig, B. H. Deng, G. Fiksel, V. Mirnov, S. C. Prager, J. S. Sarff, and V. Svidzinski, Phys. Rev. Lett. **93**, 045002 (2004).

[15] P. H. Diamond, C. J. McDevitt, Ö. D. Gürcan, T. S. Hahm, W. X. Wang, E. S. Yoon, I. Holod, Z. Lin, V. Naulin, and R. Singh, Nucl. Fusion **49**, 045002 (2009).

[16] T. S. Hahm, P. H. Diamond, O. D. Gurcan, and G. Rewoldt, Phys. Plasmas **15**, 055902 (2008).

[17] A. F. Almagri, J. T. Chapman, C. S. Chiang, D. Craig, D. J. Den Hartog, C. C. Hegna, and S. C. Prager, Phys. Plasmas **5**, 3982 (1998).

[18] J. M. Finn, P. N. Guzdar, and A. A. Chernikov, Phys. Fluids B **4**, 1152 (1992).

[19] A. B. Rechester and M. N. Rosenbluth, Phys. Rev. Lett. **40**, 38 (1978); M. N. Rosenbluth, R. Z. Sagdeev, J. B. Taylor, and G. M. Zaslavski, Nucl. Fusion **6**, 297 (1966).

[20] J. A. Reusch, J. Anderson, D. J. Den Hartog, F. Ebrahimi, D. Schnack, H. Stephens, and C. Forest, Phys. Rev. Lett. **107**, 155002 (2011).

[21] A. Kuritsyn, G. Fiksel, A. F. Almagri, D. L. Brower, W. X. Ding, M. C. Miller, V. V. Mirnov, S. C. Prager, and J. S. Sarff, Phys. Plasmas **16**, 055903 (2009).

[22] F. Ebrahimi, V. V. Mirnov, S. C. Prager, and C. R. Sovinec, Phys. Rev. Lett. **99**, 075003 (2007).

[23] J. R. King, C. R. Sovinec, and V. V. Mirnov, Phys. Plasmas **19**, 055905 (2012).